water

MDPI

Article

Study on Soil Water Infiltration Process and Model Applicability of Check Dams

Heng Wu, Shengdong Cheng *, Zhanbin Li, Ganggang Ke and Hangyu Liu

State Key Laboratory of Eco-Hydraulics in Northwest Arid Region, Xi'an University of Technology, Xi'an 710048, China; wuheng9699@163.com (H.W.); zhanbinli@162.com (Z.L.); ganggangkerum@163.com (G.K.); liuhangyu1998@163.com (H.L.)

* Correspondence: xautcsd@163.com; Tel./Fax: +86-29-61123629

Abstract: As the primary ecological construction measure on the Loess Plateau, check dams play an essential role in developing agricultural production, improving people's production and life, and replenishing groundwater. Soil water infiltration is the most important way to replenish groundwater in the dam land. In order to investigate the water infiltration process of check dams, an empirical model suitable for the simulation of the dam land infiltration process was selected. The soil water infiltration process of the check dam was studied by a field test and a model simulation. The results showed that there were few macropores in the dam, and the water mainly moved downwards in the form of matrix flow. Moreover, the stable infiltration rate of the dam site was low, and its infiltration process could be divided into three stages: rapid infiltration, fluctuating infiltration, and stable infiltration. In addition, the infiltration rate of a non-silted dense layer was 2.4~5 times that of a silted dense layer. The Horton model had a good fitting effect on the water infiltration process of the check dam and thus was suitable for the simulation and prediction of the water infiltration process of the dam. The results can provide a theoretical basis for efficient soil water utilization and infiltration simulation of check dam land.

Keywords: check dams; infiltration process; model applicability; silted dense layer

Citation: Wu, H.; Cheng, S.; Li, Z.; Ke, G.; Liu, H. Study on Soil Water Infiltration Process and Model Applicability of Check Dams. *Water* **2022**, *14*, 1814. https://doi.org/10.3390/w14111814

Academic Editor: Jan Wesseling

Received: 16 April 2022
Accepted: 2 June 2022
Published: 4 June 2022

1. Introduction

As an essential project to control soil erosion, the check dam has been widely used worldwide. China has also carried out large-scale check dam construction on the Loess Plateau [1]. The large-scale construction of check dams not only plays a role in blocking sediment and storing water, regulating runoff, and improving species richness the upstream but also increases soil infiltration, replenishes groundwater sources, increases soil water supply for grain crop growth and production, has an important impact on the underground hydrological cycle, and promotes the formation of underground reservoirs [2–5]. Soil water is the basis of plant growth and survival and an essential part of the hydrological cycle [6]. As a primary link among precipitation, soil water, and groundwater transformation, soil infiltration plays an essential role in the hydrological cycle. In addition, soil infiltration capacity is also an important index to measure soil water retention and erosion resistance [7]. Soil infiltration is one of the main ways to recharge groundwater. Especially on the Loess Plateau, soil moisture is mainly recharged by several high-intensity rainfalls in the rainy season, which is the primary source of groundwater recharge in this area [8,9].

Located in the north of central China, the Loess Plateau is one of the most vulnerable areas in China's ecosystem [10]. The annual precipitation in this area is low, and the rainfall is unevenly distributed throughout the year. Often struck by short-duration, high-intensity rainstorms in summers, the Loess Plateau is prone to severe water and soil loss [11,12]. Severe soil erosion and water loss aggravate the deterioration of the ecological environment, increasing the difficulty in soil and water loss treatment. This interaction reduces the soil fertility of the land on the Loess Plateau, thereby seriously affecting the production and

life of local people [13–15]. In order to alleviate soil erosion on the Loess Plateau and improve the living environment, China has taken a series of soil and water conservation measures, such as returning farmland to forests and grasslands, gully treatment, and check dam construction, which has significantly improved regional ecosystem and curbed soil erosion [16–18].

The unique geographical characteristics and climatic conditions of the Loess Plateau significantly affect the soil moisture in this area. The infiltration process of soil water is affected by topography, soil bulk density, texture, and initial soil water content [19,20]. Among them, soil texture has a much more significant impact on soil infiltration than topography and other factors [21]. After the completion of the check dam, due to the deposition of sediment, a silting dense layer is formed, which hinders the water movement, affects the water infiltration process, and then changes the water distribution of the dam land [22]. The dam land formed by soil deposition in the check dam has become the prominent grain-producing area of the Loess Plateau. The change in soil moisture is bound to transform the ecological construction and people's production and life in this region [23,24]. However, few studies have been carried out on the water infiltration of check dams. Therefore, understanding the process and mechanism of soil water infiltration in check dam land helps solve related ecological and environmental problems and contributes to the efficient utilization and sustainable development of water and soil resources in dam land.

With typical check dams on the Loess Plateau as the research object, this paper attempted to study the soil water infiltration mode, infiltration process, and water resistance capacity of a silted dense layer through field tests and indoor simulation. In addition, this paper fitted and evaluated the infiltration process via different infiltration models to provide a theoretical, reference, and scientific basis for understanding the infiltration process of check dam land, the ecological construction of check dams, and the efficient utilization of resources.

2. Materials and Methods

2.1. Overview of the Study Area

The study area is located at Nianyangou No. 3 Dam in Wangmaogou watershed, Suide County, Shaanxi Province (Figure 1). Wangmaogou is a branch of Jiuyuan gully, a first-class tributary on the left bank of the Wuding River. Its main gully is 3.75 km long. The surface soil of the basin is mainly composed of the Malan Loess with a fine texture and loose organization, which has poor erosion resistance. There are 23 check dams in the Wangmaogou basin, including 2 large ones, 7 medium ones, and 14 small ones, with a governance degree of 77.7%.

Nianyangou is the branch of the Wangmaogou watershed and has a drainage area of 5.97 km^2. It is located at 110°20′04″~110°22′28″ east longitude and 37°25′33″~37°35′54″ north latitude. The altitude ranges between 1027~1188 m, and the average slope is 12.5°. The basin has a temperate continental monsoon climate, with an average annual rainfall of 513 mm, and 70% of its precipitation falls from July to September. A total of 3 check dams were built in the basin, among which Nianyangou No. 3 Dam has no drainage structures. The soil texture is mainly yellow cotton soil, the soil bulk density is 1.33 ± 0.19 (g/cm^3), the silt content is 66.12 ± 4.69%, the sand content is 32.14 ± 4.72%, and the clay content is 1.73 ± 0.20%. The main crop planted in the dam land is corn.

2.2. Experimental Design and Sampling

The field test and sample collection were conducted in Nianyangou No. 3 Dam in August 2020. Due to flood scouring, the dam body of Nianyangou No. 3 dam has been damaged. There is a breach and erosion upstream. In order to facilitate the test and monitor, the field in situ test point was set at the dam site around the breach. The in situ field test mainly included the bright blue staining and double-ring infiltration tests. The bright blue staining test determines whether there is preferential flow in the dam site infiltration. The

double-ring infiltration experiment explores the water infiltration process of dam land and the water-blocking capacity of the silted dense layer. The location of the soil sample collection point is consistent with the double-ring infiltration test point.

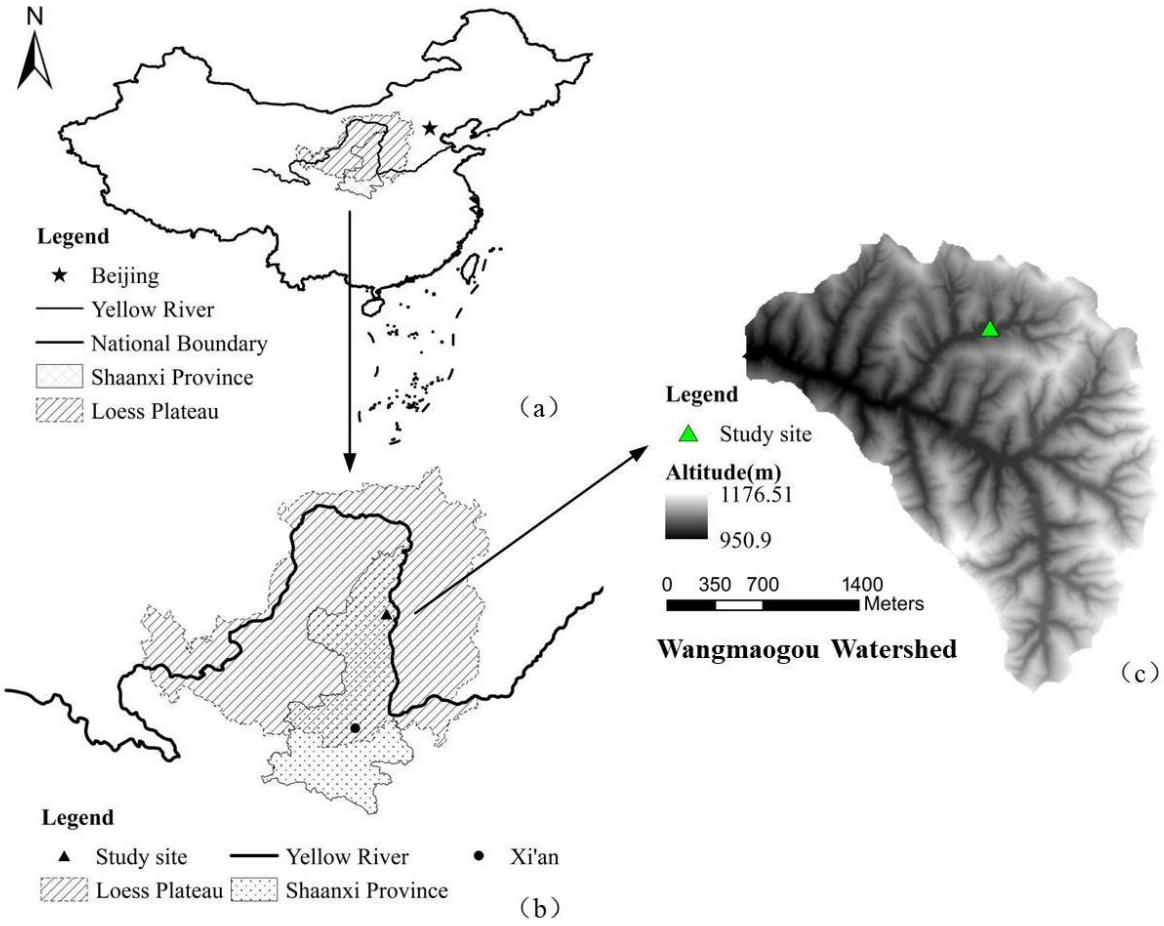

Figure 1. Location of the Loess Plateau in China (**a**); Location of the study site on the Loess Plateau (**b**); Wangmaogou Watershed Digital Elevation Model and location of the study site (**c**).

(1) Bright blue dyeing experiment

A square block with an area of 1 square meter was drawn in the test area. After removing the surface floating soil and litter and leveling the quadrat, iron sheets with a length and width of 1 m and a height of 30 cm were vertically buried into the ground for 20 cm around the sample plot. Then, the soil around the iron sheet was tamped with a rubber hammer to prevent the reagent solution from dripping down the iron sheet. Subsequently, the sample plot was sprayed with a 20 L bright blue solution with a concentration of 4 g/L, which was then tightly covered with a plastic sheet to prevent the influence of precipitation. Moreover, 24 h later, the iron sheets around the sample plot were removed carefully while not affecting the soil in the sample plot. After that, the soil within 10 cm of the edge of the sample plot was removed to reduce the possible abnormal infiltration of dye around the iron sheets. Subsequently, a soil section with a depth of 80 cm was excavated and leveled, and then the vertical soil profile was photographed and recorded with a camera (Figure 2). The camera was 1.2 m away from the soil section, the focal length was set to 28 mm, and the picture was stored in Jpg format. To avoid contingency, we set up two parallel tests, marked as a and b.

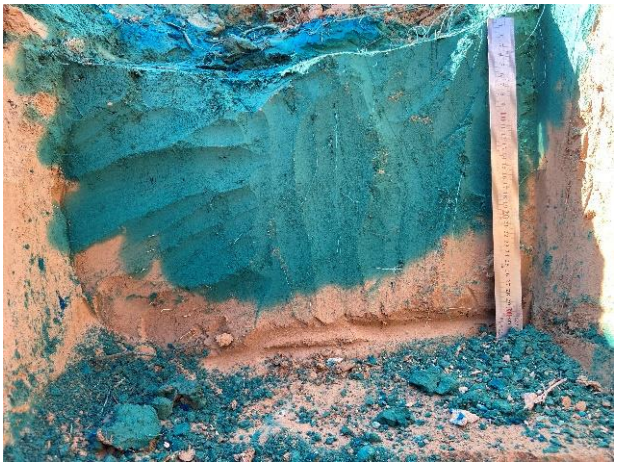

Figure 2. Photographs of the experiment.

Among the indices describing the morphological characteristics of soil water infiltration, the dyeing area ratio is the most widely used. This indicator mainly describes the proportion of the number of soil pixels stained by the dyeing reagent in the whole soil profile along the vertical direction. When the dyeing area exceeds 75%, it indicates that the soil water in the dyeing area mainly comprises matrix flow. In comparison, when it is below 25%, the soil water in the area is mainly transported via preferential flow [25]. The dyeing area ratio is calculated by:

$$D_s = \frac{D_i}{D_i + N_i} \tag{1}$$

where D_s is the dyeing area ratio (%); D_i is the number of stained pixels at depth i(pixel); N_i is the number of undyed pixels at depth i(pixel); i is the number of vertical pixels of the image (pixel).

(2) Double-ring infiltration experiment

Before the test, the test site was cleared of floating soil and vegetation litter and leveled. Then the inner and outer rings with a height of 20 cm were struck into the leveled site. The diameters of the inner and outer rings were 25 and 50 cm, respectively. Two Markov bottles with a capacity of 5 L were used to provide water to the two rings, respectively. The infiltration volumes of the rings were recorded every 5 min. After the infiltration volume became stable, the recording time was extended. During the infiltration process, the water surfaces of the inner and outer rings were maintained at the same height to ensure vertical water infiltration into the inner ring and to reduce the transverse seepage flow. A total of 17 double-ring infiltration tests were carried out, of which 15 were used to determine the soil water infiltration characteristics of the dam site, and two were mainly carried out for the silted dense layer, recorded as A and B, in order to study the water-blocking effect of the silted dense layer. Every three tests were conducted simultaneously as a group, with a distance of 1 m for each test, 2 m for each group, and 10 m for the infiltration test points of the silted dense layer. In the infiltration test on the silted dense layer, the CS616 soil moisture sensor probe from Campbell of the United States was inserted into the silted dense layer and its upper and lower parts to monitor the water infiltration through the siltation layer. The equipment includes ten soil moisture sensor probes, numbered 1~10. The Campbell CS616 soil moisture sensor uses the highly sensitive time domain reflectometry to measure the moisture content of soil or other porous media, with a measurement accuracy of ±2.5%.

The infiltration rate is calculated by:

$$V_t = \frac{(Q_t - Q_{t-1}) \times 10}{S \times \Delta t(0.7 + 0.03T)} \tag{2}$$

where V_t is the soil vertical infiltration rate at time t under a certain temperature (mm/min); Q_t is the cumulative water supply of Markov bottle at time t (cm^3); Q_{t-1} is the cumulative water supply of Markov bottle at time $t-1$ (cm^3); S is the area of double ring inner ring (cm^2); Δt t is the average water temperature in a certain period (°C).

The thickness and distribution of the silted dense layer in the test soil profile were measured on-site before the test. The distribution of soil particles in the silted dense layer shows the distribution characteristics from fine particles to coarse particles from the top to the bottom. However, because the soil texture and thickness of the silted dense layer, formed by the carrying of sediment from each rainfall–runoff, are affected by many factors, such as rainfall intensity, rainfall, topographic and geomorphic characteristics, and vegetation coverage, a complete and precise coarse and fine distribution may not be formed. When recording the distribution of the silted layer, the adjacent sediment layer with mud above and sand below was regarded as the same layer, which was called the silted dense layer as a whole.

2.3. Infiltration Model

The infiltration process of this test is fitted by Philip formula [26], Kostiakov formula [27], and Horton formula [28]. The model equations are as follows:

Philip formula:

$$I(t) = 0.5St^{-1/2} + i_c \quad (3)$$

where $I(t)$ is the infiltration rate (mm/min); S is the moisture absorption rate of soil ($mm/min^{1/2}$) and it is closely related to soil's characteristics; t is infiltration time (min); i_c is the stable infiltration rate (mm/min); S and i_c can be measured by the infiltration test.

Kostiakov formula:

$$I(t) = kt^{-a} \quad (4)$$

where $I(t)$ is the infiltration rate (mm/min); t is infiltration time (min); k is the infiltration coefficient; a is the infiltration index; k and a can be obtained by fitting the experimental data;

Horton formula:

$$I(t) = i_c + (i_1 - i_c)e^{-ct} \quad (5)$$

where $I(t)$ is the infiltration rate (mm/min); i_c is the stable infiltration rate (mm/min); i_1 is the initial infiltration rate (mm/min); e is a constant with the value of 2.71828183; t is infiltration time (min); c is the empirical constant, which represents the attenuation rate of infiltration rate from initial to stable.

2.4. Sample Collection

The samples were obtained from the test soil profile (0~100 cm) at 10 cm in the Nianyangou No. 3 dam. from August to September 2020. The ring knife (100 cm^3) method measured the soil bulk density. In addition, we took out part of the soil and put it into self-sealing bags for sealing. The wet weight of the soil samples was measured on-site, and then the samples were taken to the laboratory for drying at 105 °C. After drying, we measured the soil texture, bulk density, and water content. Samples from each layer had three duplicates.

2.5. Data Calculation and Processing

In order to avoid distortion of the original image caused by human and environmental factors, Photoshop CS6 and Image-Pro Plus 6.0 were applied to correct, cut, binarize, and reduce noises. The rest of the data were processed by Excel 2010 for data statistics, SPSS 22.0 for correlation analysis, and origin 2017 for mapping.

3. Results

3.1. Dam Soil Infiltration Mode

The staining results of the vertical soil profile are shown in Figure 3. The blue is the staining area, and white is the non-staining area. The results of the two dyeing tests are

similar. The distribution of the dye was relatively uniform along the vertical direction, and the distribution of the bottom wetting front of the two tests was relatively smooth without any apparent protrusion.

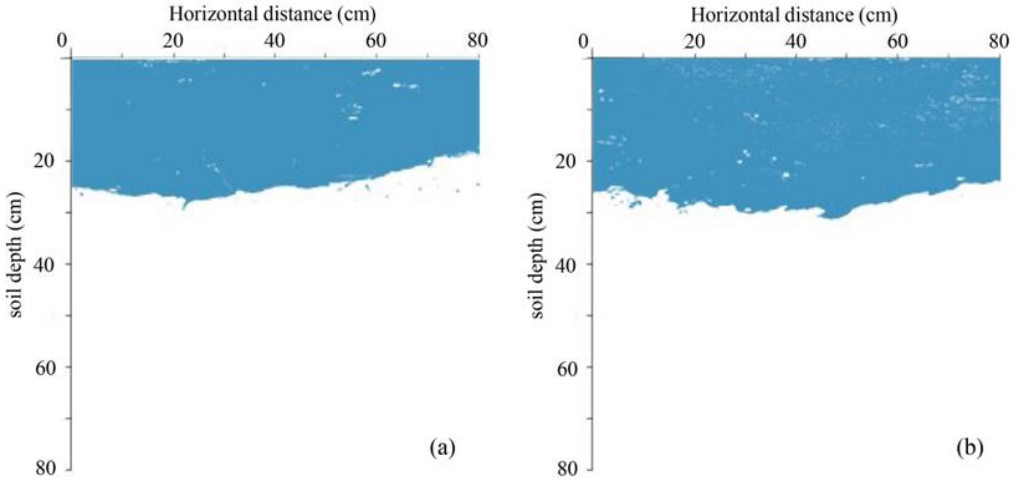

Figure 3. The vertical soil profiles. (**a**) is the result of the first dam site profile dyeing test; (**b**) is the result of the second dam site profile dyeing test.

To further determine the soil water infiltration mode of the dam land, the vertical distribution of the dyeing area ratio of the dam land was analyzed (Figure 4). The more profound dyeing depth reached about 33 cm in the two dam land dyeing tests. Within the depth range of 0~25 cm, the proportion of the dyeing area was relatively stable; for both of the tests it was over 80%, and the maximum reached 100 and 98%, respectively. The proportion of the staining area plunged within the depth range of 25~33 cm and finally stabilized at zero.

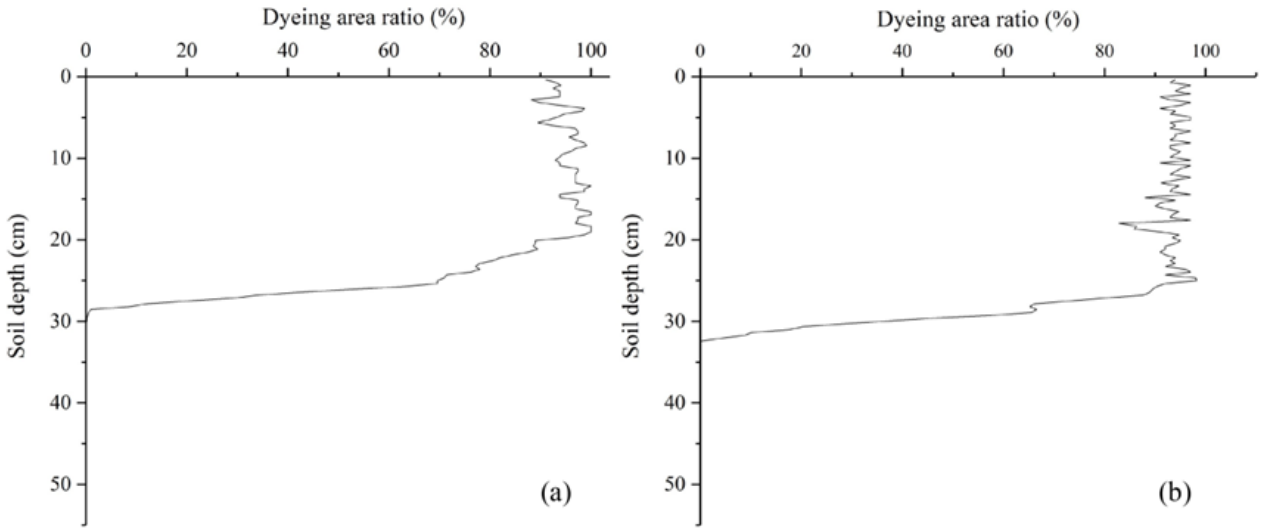

Figure 4. Distribution of dyeing area ratio. (**a**) is the dyeing area ratio result of the first dam section dyeing test, and (**b**) is the dyeing area ratio result of the second dam section dyeing test.

3.2. Infiltration Characteristics of Dam Soil

Initial infiltration rate, stable infiltration rate, and cumulative infiltration are critical soil water infiltration capacity indicators. The infiltration characteristics of the dam site infiltration test are shown in Table 1. The infiltration rate of each test was stable after 90 min of infiltration. Thus, only the cumulative infiltration amount at the first 90 min of each test was used to characterize the infiltration capacity of the dam in the early stage of infiltration.

The initial infiltration rate ranged from 0.81 to 2.00 mm/min. The stable infiltration rate ranged from 0.39 to 1.08 mm/min. The average infiltration rate varied from 0.43 to 1.23 mm/min. Cumulative infiltration in the first 90 min was 3.91~11.71 cm. The variation trend of the infiltration rate of the dam site infiltration test was the same (Figure 5): the initial infiltration rate was high. Then the infiltration rate fluctuated and decreased, and finally tended to be stable with the increasing infiltration time.

Table 1. Characteristics of soil water infiltration.

Infiltration Characteristics	Test Times				
	1	**2**	**3**	**4**	**5**
i_1	1.83	1.59	2.00	1.59	0.81
i_c	0.87	1.08	0.51	0.53	0.39
i_a	1.03	1.23	0.66	0.60	0.43
F	9.43	11.71	6.17	5.38	3.91

i_1 = initial infiltration rate (mm/min); i_c = stable infiltration rate (mm/min); i_a = average infiltration rate (mm/min); F = cumulative infiltration amount in the first 90 min (cm).

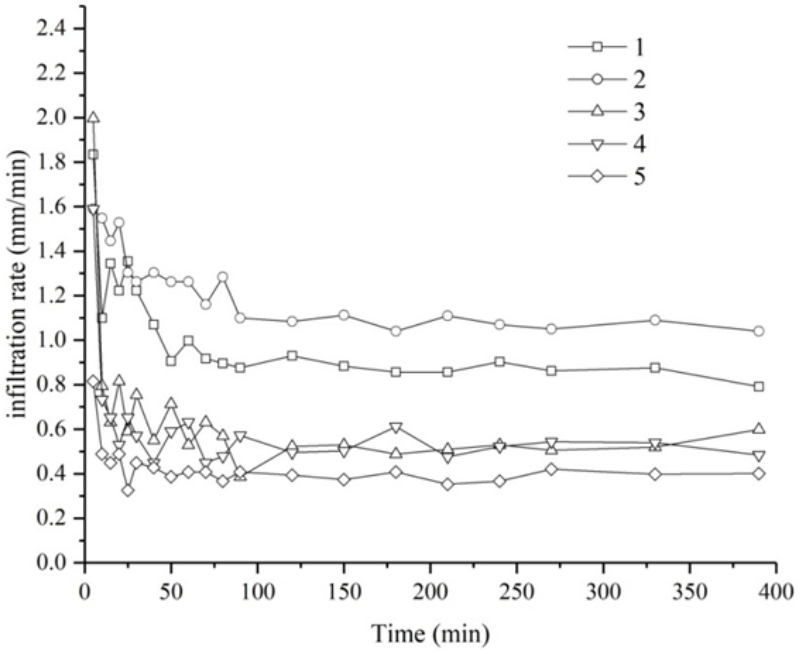

Figure 5. Variation characteristics of soil water infiltration rate.

3.3. Water-Blocking Capacity of Silted Dense Layer

Two infiltration tests were performed on the silted dense layer, A and B. Site A was close to the dam body, and Site B was far away from the dam body. The distance between the two sites was 10 m. Before the test, the distribution of silted dense layer within 1 m depth of each test site was counted respectively (Figure 6). The silted dense layer at the 28 cm depth of Figure 6B was composed of coarse and fine particles, which were mainly silted by the sediment carried by a rainstorm. Hence, it was also regarded as a silted dense layer. There are apparent differences in the silted dense layer's depth, thickness, and quantity.

In this study, the initial water content was the soil water content, which was monitored by the water probe before the test (Table 2). It can be seen from the Table that the soil water content of the silted dense layer monitored by each probe was significantly higher than those in other locations, and the soil water content of the silted dense layer in the same profile was up to 3.23 times that of the non-silted dense layer. At the same time, the soil

water content near the upper part of the silted dense layer was generally higher than that at the lower part.

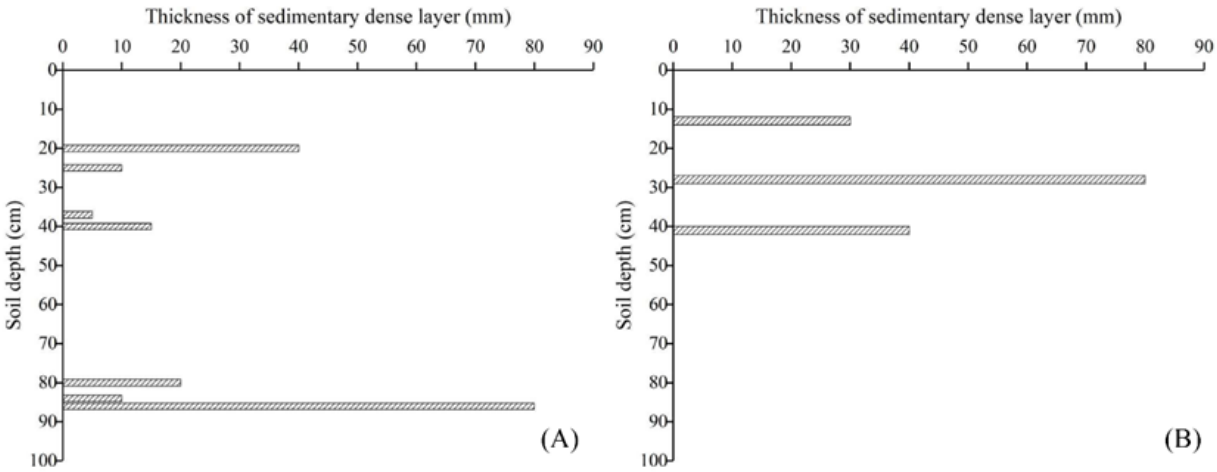

Figure 6. The vertical distribution of the sedimentary dense layer. (**A**) is the distribution of silted dense layer in the first silted dense layer infiltration test, (**B**) is the distribution of silted dense layer in the second silted dense layer infiltration test.

Table 2. Initial soil water statistics.

A				B			
Probe Number	**Soil Depth (cm)**	**Soil Water Content (%)**	**Sedimentation Dense Layer**	**Probe Number**	**Soil Depth (cm)**	**Soil Water Content (%)**	**Sedimentation Dense Layer**
1	10	20.8	No	1	12	34.6	No
2	20	43.7	Yes	2	15	44	Yes
3	23	42.5	Yes	3	16	43	Yes
4	35	19.5	No	4	27	32.7	No
5	42	27.9	No	5	31	31.5	Yes
6	57	23.7	No	6	37	21.6	No
7	72	16.4	No	7	40	26	No
8	81	35	Yes	8	43	48.8	yes
9	86	45.7	Yes	9	46	20.7	No
10	91	52.7	yes	10	53	21.8	No

The soil moisture probe obtains the change process of soil water content at different depths during the infiltration test of the silted dense layer (Figure 7). The results of two experiments, Figure 7A,B, showed that surface soil water content changed sharply, and the soil water content of deep soil was relatively stable without an apparent change. When the soil probe detected a water content change of more than 1%, the water was considered to have migrated here. Based on this, the infiltration rates of water migration through the dense layer and non-silted dense layer were calculated. The maximum infiltration rate of the dense layer near the surface was 5 mm/min, and the infiltration rate dwindled with the increasing depth, with a minimum of 0.18 mm/min. The infiltration rate of the non-silted dense layer also peaked near the surface, 12 mm/min. It decreased with the rising depth, with a minimum of 0.8 mm/min. It can be concluded that the infiltration rate of a non-silted dense layer was 2.4~5 times that of the silted dense layer.

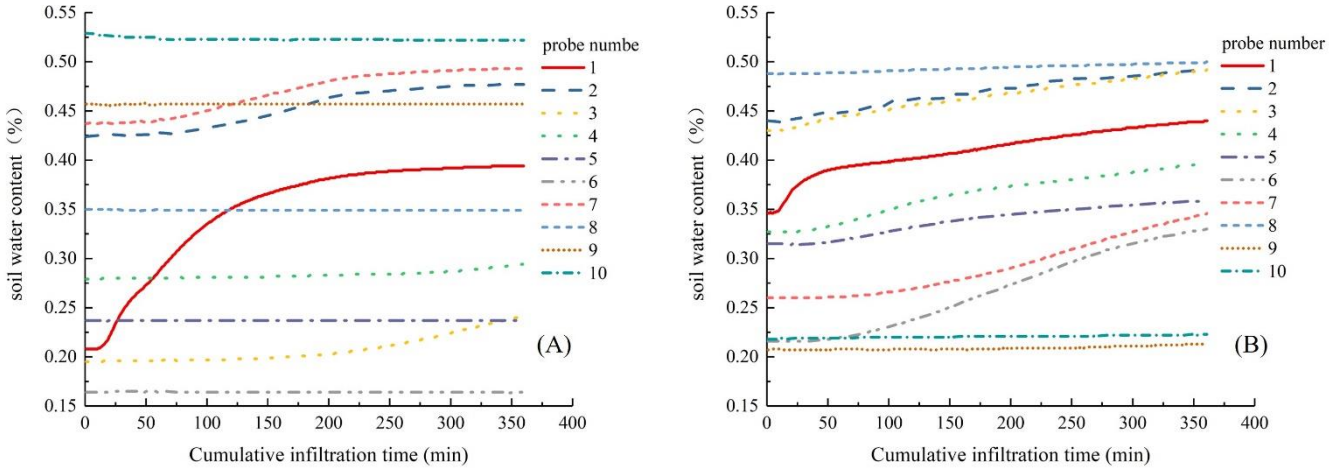

Figure 7. Dynamic change of soil water content. (**A**) is the change of water content of each probe with time in the first siltation dense layer infiltration test, (**B**) is the change of water content of each probe with time in the second siltation dense layer infiltration test.

3.4. Influencing Factors of Soil Infiltration Characteristics in the Dam Site

The correlation analysis found that the correlation between infiltration characteristics and influencing factors is insignificant, and the relationship between infiltration rate and influencing factors in different infiltration stages is different (Table 3). The initial infiltration rate negatively correlates with silt, clay, initial water content, and bulk density, yet a positive correlation with sand. The stable infiltration rate and average infiltration rate are negatively correlated with sand, clay, and bulk density but positively correlated with silt and initial water content.

Table 3. Correlation analysis between soil infiltration characteristics and soil properties.

Soil Index	Initial Infiltration Rate	Stable Infiltration Rate	Average Infiltration Rate	Silt	Sand	Clay	Initial Moisture Content	Bulk Density
Initial infiltration rate	1							
Stable infiltration rate	0.332	1						
Average infiltration rate	0.440	0.989 **	1					
Silt	−0.442	0.365	0.284	1				
Sand	0.456	−0.351	−0.268	−0.999 **	1			
Clay	−0.421	−0.261	−0.318	0.172	−0.214	1		
Initial moisture content	−0.628 *	0.252	0.173	0.824 **	−0.830 **	0.298	1	
Bulk density	−0.084	−0.286	−0.259	0.011	−0.026	0.348	0.074	1

Note: ** indicates significant correlation at 0.01 level bilateral; * indicates significant correlation at 0.01 level bilateral.

3.5. Simulation of Soil Water Infiltration Process in Dam Land

In order to verify the applicability of different infiltration models to the simulation of the dam land infiltration process, three classical infiltration models were used for this research, and the accuracy of the model was evaluated by statistical parameters such as determination coefficient (R^2) and root mean square error (RMSE). The fitting parameters and evaluation results of the infiltration model for the dam infiltration process are shown in Table 4. The closer the determination coefficient R^2 is to one, the smaller the root mean square error RMSE, indicating that the better the fitting effect of the model. Among them, the average R^2 of the Philip model, Kostiakov model, and Horton model are 0.72, 0.63, and 0.77, respectively, and the corresponding average RMSEs are 0.11, 0.12, and 0.10, respectively. The RMSEs of the three models are similar. The results show that the three models can reflect the water infiltration process of dam land, and the fitting accuracy is in the descending trend of Horton > Philip > Kostiakov. This result shows that Horton has the best fitting effect and a strong applicability for the water infiltration process of dam land

and thus can be used for the simulation and prediction of the water infiltration process in dam land.

Table 4. Model parameters of the Philip, Kostiakov, and Horton models for simulation of soil water infiltration.

Test Times	Philip Model				Kostiakov Model				Horton Model				
	S	i_c	R^2	*RMSE*	k	c	R^2	*RMSE*	a	i_c	i_1	R^2	*RMSE*
1	4.55	0.70	0.83	0.10	2.10	0.17	0.77	0.11	0.04	0.87	1.83	0.79	0.11
2	3.24	0.99	0.85	0.07	1.93	0.11	0.89	0.05	0.02	1.06	1.59	0.90	0.05
3	5.42	0.26	0.67	0.18	2.49	0.34	0.57	0.21	0.10	0.53	2.00	0.72	0.17
4	3.86	0.32	0.62	0.14	1.65	0.25	0.48	0.17	0.10	0.52	1.59	0.73	0.12
5	1.6	0.31	0.64	0.06	0.75	0.14	0.45	0.07	0.09	0.39	0.81	0.73	0.05

S = soil sorptivety; i_c = stable infiltration rate (mm/min); *RMSE* = root mean square error; c, k and a = empirical coefficients; i_1 = initial infiltration rate (mm/min).

4. Discussion

4.1. Analysis on Infiltration Mode and Process of Dam Soil

The dam land was mainly formed by the sediment deposition generated by the interception of precipitation runoff by the dam body. The soil would become more compact and denser during the interception and redistribution of sediment particles [29]. Since the pores in the soil were small, it was difficult for water to infiltrate the soil layer of the dam. At the same time, the top part of the soil water infiltration and migration formed an obvious boundary with the original soil, i.e., the wetting front. At this time, the soil water gradient at the wetting front was large. Consequently, the water migration rate here was more significant than that at other locations in the same horizontal direction, resulting in a sharp decline in the staining area ratio to zero. Therefore, the migration form of preferential flow was not shown in the migration process of water in the dam, and the dam water mainly moved downwards in the form of matrix flow.

In the beginning, the soil water content was low, and the soil water suction was large. In this study, the water seeped into the soil rapidly under the combined action of gravity and soil water suction. This stage, therefore, was the rapid infiltration stage. Since then, the surface soil water content has increased rapidly. According to the principle of soil water potential, when the soil water content increases, the soil water suction will decrease. Therefore, the infiltration rate would plunge when the surface water content reached a certain amount. At the same time, due to the influences of soil pores and other factors, the infiltration rate would fluctuate. Thus, this stage was the fluctuating infiltration stage. After a while, when the soil pores were filled with water, the soil water suction dropped to the lowest, and the water only moved downwards under the action of gravity. At this time, the water infiltration gradually stabilized and finally reached a stable infiltration rate. This stage, therefore, was the stable infiltration stage. Similarly, the infiltration process of dam land could also be roughly divided into three stages: rapid infiltration (0~20 min), fluctuating infiltration (20~90 min), and stable infiltration (after 90 min).

4.2. Analysis of the Water-Blocking Capacity of Silted Dense Layer

Due to the energy loss in the transport process of sediment particles in the check dam, the transport distances of sediment particles were different, which eventually led to the difference in the thickness and quantity of silted dense layers. This result is consistent with the research results of Zhang [30]. When the water reached the dense layer, it was greatly hindered. Consequently, the water was forced to move laterally. In this case, the soil water content in the upper part of the dense layer began to increase gradually. In contrast, the water in the lower part took a long time to pass through the dense layer due to the higher water-holding capacity and water resistance of the dense layer. Thus, the soil water content in the lower part of the dense layer was low. At the same time, through the field investigation of the silted dense layer, the dense layer sometimes had

mixed deposits of coarse and fine particles. Due to the existence of a small amount of coarse-grained soil in the dense layer, there were tiny pores in the dense layer, forming a short preferential flow channel, and a wetting front crossed the dense layer to reach the lower soil first. Therefore, the deep-water content in Figure 7A changes earlier than the surface water. With the increasing soil depth, the water content passing through the dense layer and the non-silted dense layer gradually decreased. However, the water transport rate of the dense layer was still significantly lower than that of the non-silted dense layer. Therefore, it was determined that the silted dense layer has the function of holding water and hindering water movement.

4.3. Analysis of the Influencing Factors of Soil Infiltration Characteristics in the Dam Site

Soil moisture is affected by many factors, such as soil texture and soil water content during infiltration [31]. In the research results, the relationship among stable infiltration rate, average infiltration rate, and initial water content is contrary to previous research results [32]. This result is mainly because of the formation of silt dams. The coarse sand will silt before the fine sand, resulting in dense silt layers with different thicknesses in the soil and further different influencing factors of infiltration rate in different infiltration stages [33]. It can be seen that the water infiltration process of the dam site was affected by factors such as the soil texture and soil water content, as well as by those related to the silted dense layer, such as the thickness of the dense layer and the distance from the surface layer.

4.4. Applicability Analysis of Infiltration Model

The soil water infiltration process is one of the critical processes of water transformation [34]. With the construction of large-scale ecological projects on the Loess Plateau and the continuous enhancement of ecological quality, analyzing and predicting the infiltration process of check dam land is of great significance to improve the utilization efficiency of water and soil resources in the dam land [35]. The fitting results of three different infiltration models showed that the Horton model could better fit the soil water infiltration process of the check dam than the other two models. The infiltration rate of the Kostiakov model is infinite at the initial time. Nevertheless, when the time tends to infinity, the infiltration rate trends to zero, which is inconsistent with the actual infiltration process. The water infiltration rate will eventually tend to stabilize at a certain constant and cannot be zero, so the predicted value will be low in an application. Field test data have verified the effect of the Philip model. However, this model was proposed under the condition of homogeneous soil, surface ponding, and the uniform distribution of initial water content [36,37]. Therefore, when it is applied to simulate the infiltration process of dam land with prominent soil stratification characteristics, there will be some errors, resulting in poor fitting accuracy. Although the fitting accuracy of the Philip model was not as good as that of the Horton model, its parameters were more in line with the actual water infiltration theory [38]. In the actual infiltration process, due to the existence of gravity potential, the infiltration rate will eventually tend to be stable [39].

Moreover, the constant term in the Horton model can reflect that the infiltration reaches stability under the action of gravity, so the fitting effect of the Horton model is better. In addition, the fitting accuracy of the model is also affected by soil structure, organic matter content, porosity, and other factors [40]. Therefore, the applicability study of the infiltration process of the dam land on the Loess Plateau through the field in-situ observation experiment and infiltration model provides an essential theoretical basis for improving the infiltration model.

5. Conclusions

(1) The number of macropores in the soil of the check dam is small, and the water mainly moves downward in the form of matrix flow, without preferential flow. Its

infiltration process is similar to the normal, divided into three stages: rapid infiltration, fluctuating infiltration, and stable infiltration.

(2) The silted dense layer can store water and hinder the downward movement of water. In the same profile, the soil water content in the silted dense layer is higher than that in the non-silted dense layer, and the infiltration rate is significantly lower than that in the non-silted dense layer. The maximum water content of the silted dense layer is 3.23 times that of the non-silted dense layer, and the infiltration rate of the non-silted dense layer is 2.4~5 times that of the silted dense layer.

(3) The Horton model, Philip model, and Kostiakov model can be applied to simulate the water infiltration process of dam land. The Horton model outperforms the other two models' in terms of accuracy and can provide a reference for the future simulation of dam land water infiltration.

In general, water-holding and water-blocking properties in the silted dense layer are of great significance to the slow and continuous replenishment of groundwater resources in check dams. It is also an important reason for forming soil reservoirs in check dams.

Author Contributions: H.W., S.C. and Z.L. conceived the main idea of the paper. H.W., G.K. and H.L. designed and performed the experiment. H.W. wrote the manuscript and all authors contributed in improving the paper. All authors have read and agreed to the published version of the manuscript.

Funding: This research was supported by the National Natural Science Foundation of China (U2040208), the National Natural Science Foundation of China (52179043, 52009104).

Institutional Review Board Statement: Not applicable.

Informed Consent Statement: Not applicable.

Data Availability Statement: Not applicable.

Acknowledgments: We thank the reviewers for their useful comments and suggestions.

Conflicts of Interest: The authors state that they have no known competing financial interests or personal relationships that could affect the work described in this article.

References

1. Zhang, Y.; Li, P.; Liu, X.J.; Xiao, L.; Shi, P.; Zhao, B.H. Effects of farmland conversion on the stoichiometry of carbon, nitrogen, and phosphorus in soil aggregates on the Loess Plateau of China. *Geoderma* **2019**, *351*, 188–196. [CrossRef]
2. Wang, T.; Li, P.; Li, Z.B.; Hou, J.M.; Xiao, L.; Ren, Z.P.; Xu, G.C.; Yu, K.X.; Su, Y.Y. The effects of freeze–thaw process on soil water migration in dam and slope farmland on the Loess Plateau, China. *Sci. Total Environ.* **2019**, *666*, 721–730. [CrossRef] [PubMed]
3. Wang, T.; Hou, J.M.; Li, P.; Zhao, J.H.; Li, Z.B.; Matta, E.; Ma, L.P.; Hinkelmann, R. Numerical simulation of check dams impacts on flood characteristics in a small catchment on the Loess Plateau, China. *Nat. Hazards* **2021**, *105*, 059–3077. [CrossRef]
4. Bai, L.C.; Jiao, J.Y.; Wang, N.; Chen, Y.L. Structural Connectivity of Sediment Affected by Check Dams in Loess Hilly-Gully Region, China. *Water* **2021**, *13*, 2644. [CrossRef]
5. Wang, Z.Y.; Chen, Z.Y.; Yu, S.; Zhang, Q.; Wang, Y.; Hao, J.W. Erosion-control mechanism of sediment check dams on the Loess Plateau. *Int. J. Sediment Res.* **2021**, *36*, 668–677. [CrossRef]
6. Corradini, C. Soil moisture in the development of hydrological processes and its determination at different spatial scales. *J. Hydrol.* **2014**, *516*, 1–5. [CrossRef]
7. Gwak, Y.; Kim, S. Factors affecting soil moisture spatial variability for a humid forest hillslope. *Hydrol. Process.* **2017**, *31*, 431–445. [CrossRef]
8. Suo, L.Z.; Huang, M.B.; Zhang, Y.K.; Duan, L.X.; Shan, Y. Soil moisture dynamics and dominant controls at different spatial scales over semiarid and semi-humid areas. *J. Hydrol.* **2018**, *562*, 635–647. [CrossRef]
9. Wang, S.; Fu, B.J.; Gao, G.Y.; Liu, Y.; Zhou, J. Responses of soil moisture in different land cover types to rainfall events in a re-vegetation catchment area of the Loess Plateau, China. *Catena* **2013**, *101*, 122–128. [CrossRef]
10. Li, Z.S.; Yang, L.; Wang, G.L.; Hou, J.; Xin, Z.B.; Liu, G.H.; Fu, B.J. The management of soil and water conservation in the Loess Plateau of China: Present situations, problems, and counter-solutions. *Acta Ecol. Sin.* **2019**, *39*, 7398–7409.
11. Wang, T.; Li, P.; Liu, Y.; Hou, J.M.; Li, Z.B.; Ren, Z.P.; Cheng, S.D.; Zhao, J.H.; Hinkelmann, R. Experimental investigation of freeze-thaw meltwater compound erosion and runoff energy consumption on loessal slopes. *Catena* **2020**, *185*, 104310. [CrossRef]
12. Cheng, S.D.; Hang, P.L.; Li, P.; Cheng, Y.T.; Guo, M.J. Effects of terracing on the slope stability in the rocky mountain area of southern shaanxi province. *Res. Soil Water Conserv.* **2018**, *25*, 157–161. (In Chinese with English abstract)

13. Chen, Y.P.; Wang, K.B.; Lin, Y.S.; Shi, W.Y.; Song, Y.; He, X.H. Balancing green and grain trade. *Nat. Geosci.* **2015**, *10*, 739–741. [CrossRef]
14. Liang, W.; Bai, D.; Wang, F.Y.; Fu, B.J.; Yan, J.P.; Wang, S.; Yang, Y.T.; Long, D.; Feng, M.Q. Quantifying the impacts of climate change and ecological restoration on streamflow changes based on a Budyko hydrological model in China's Loess Plateau. *Water Resour. Res.* **2015**, *51*, 6500–6519. [CrossRef]
15. Liu, G.B.; Shanguan, Z.P.; Yao, W.Y.; Yang, Q.K.; Zhao, M.J.; Dang, X.H.; Guo, M.H.; Wang, G.L.; Wang, B. Ecological effects of soil conservation in Loess Plateau. *Bull. Chin. Acad. Sci.* **2017**, *32*, 11–19. (In Chinese with English abstract)
16. Parimalarenganayaki, S.; Elango, L. Assessment of effect of recharge from a check dam as a method of Managed Aquifer Recharge by hydrogeological investigations. *Environ. Earth Sci.* **2015**, *73*, 5349–5361. [CrossRef]
17. Ma, L.; Ni, Y.X.; Lv, X.Z.; Zhang, Q.F.; Liu, L.N. Study on relationship between underlying surface of typical warping dam and erosion and sediment yield. *IOP Conf. Ser. Earth Environ. Sci.* **2021**, *687*, 012060.
18. Tang, H.L.; Ran, Q.H.; Gao, J.H. Physics-Based Simulation of Hydrologic Response and Sediment Transport in a Hilly-Gully Catchment with a Check Dam System on the Loess Plateau, China. *Water* **2019**, *11*, 1161. [CrossRef]
19. Huang, X.; Shi, Z.H.; Zhu, H.D.; Zhang, H.Y.; Ai, L.; Yin, W. Soil moisture dynamics within soil profiles and associated environmental controls. *Catena* **2016**, *136*, 189–196. [CrossRef]
20. Hu, G.J.; Tian, L.M.; Zhao, L.; Wu, X.D.; Li, R.; Wu, T.H.; Zhu, X.F.; Du, E.J.; Wang, Z.W.; Hao, J.M.; et al. Soil infiltration processes of different underlying surfaces in the permafrost region on the Tibetan Plateau. *Hydrol. Sci. J.* **2018**, *63*, 1733–1744. [CrossRef]
21. Gao, X.D.; Wu, P.T.; Zhao, X.N.; Shi, Y.G.; Wang, J.W.; Zhang, B.Q. Soil moisture variability along transects over a well-developed gully in the Loess Plateau, China. *Catena* **2011**, *87*, 357–367. [CrossRef]
22. Yuan, S.L.; Li, Z.B.; Chen, L.; Li, P.; Zhang, Z.Y.; Zhang, J.Z.; Wang, A.N.; Yu, K.X. Effects of a check dam system on the runoff generation and concentration processes of a catchment on the Loess Plateau. *Int. Soil Water Conserv. Res.* **2022**, *10*, 86–98. [CrossRef]
23. Zhao, G.J.; Kondolf, G.M.; Mu, X.M.; Han, M.W.; Zhong, H.; Rubin, Z.; Wang, F.; Gao, P.; Sun, W.Y. Sediment yield reduction associated with land use changes and check dams in a catchment of the Loess Plateau, China. *Catena* **2017**, *148*, 126–137. [CrossRef]
24. MMongil-Manso, J.; Díaz-Gutiérrez, V.; Navarro-Hevia, J.; Espina, M.; San Segundo, L. The role of check dams in retaining organic carbon and nutrients. A study case in the Sierra de vila mountain range (Central Spain). *Sci. Total Environ.* **2018**, *657*, 1030–1040. [CrossRef]
25. Sheng, F.; Fang, Y. Study on preferential soil water flow using lodine-starch staining method. *Soils* **2012**, *44*, 144–148. (In Chinese with English abstract)
26. Wang, J.K.; Guo, Y.F.; Qi, W.; Yao, Y.F.; Wang, H. Study on horizontal infiltration law and model test of pisha sandstone soil. *J. Irrig. Drain.* **2020**, *39*, 117–121. (In Chinese with English abstract)
27. Li, H.Z.; Fan, G.S. A comparative analysis and study on forecast precision of parameters of kostiakov infiltration models. *Water Sav. Irrig.* **2017**, *11*, 27–30. (In Chinese with English abstract)
28. Al Maimuri, N.M. Applicability of Horton model and recharge evaluation in irrigated arid Mesopotamian soils of Hashimiya, Iraq. *Arab. J. Geosci.* **2018**, *11*, 610. [CrossRef]
29. Li, M.; Yang, E.; Li, P.; Bao, H.Z.; Kong, X.B.; Shen, Z.Z.; Wei, G.J. Study on the composition and changeable characteristic of sediment particle size in check dam system. *J. Basic Sci. Eng.* **2018**, *26*, 746–756. (In Chinese with English abstract)
30. Zhang, Y.; Li, P.; Liu, X.J.; Xiao, L.; Li, Z.N.; Wu, H.; Zhou, S.X.; Ren, M.X. Tracer elements revealed the soil organic carbon sources in a dam-controlled watershed. *Soil Tillage Res.* **2022**, *216*, 105184. [CrossRef]
31. Liu, Y.; Cui, Z.; Huang, Z.; López-Vicente, M.; Wu, G.L. Influence of soil moisture and plant roots on the soil infiltration capacity at different stages in arid grasslands of China-ScienceDirect. *Catena* **2019**, *182*, 104147. [CrossRef]
32. Wu, G.L.; Liu, Y.; Yang, Z.; Cui, Z.; Deng, L.; Chang, X.F.; Shi, Z.H. Root channels to indicate the increase in soil matrix water infiltration capacity of arid reclaimed mine soils. *J. Hydrol.* **2017**, *546*, 133–139. [CrossRef]
33. Zhao, G.; Klik, A.; Mu, X.; Wang, F.; Gao, P.; Sun, W. Sediment yield estimation in a small watershed on the northern Loess Plateau, China. *Geomorphology* **2015**, *241*, 343–352. [CrossRef]
34. Cao, J.H.; Chen, P.P.; Gao, X.D.; Zou, Q.F.; Fang, Y.J.; Gu, X.B.; Zhao, X.N.; Li, Y.N. Effects of plastic film residue and emitter flow rate on soil water infiltration and redistribution under different initial moisture content and dry bulk density. *Sci. Total Environ.* **2021**, *807*, 151381.
35. Shi, P.; Li, P.; Li, Z.; Sun, J.; Wang, D.; Min, Z. Effects of grass vegetation coverage and position on runoff and sediment yields on the slope of Loess Plateau, China. *Agric. Water Manag.* **2022**, *259*, 107231. [CrossRef]
36. Wang, X.Y.; Liao, W.H.; Song, P.B.; Zhang, Y.B.; Lei, X.H.; Wu, D.D. Research on the Field-scale soil infiltration law and spatial variability. *China Rural Water Hydropower* **2020**, *448*, 105–109. (In Chinese with English abstract)
37. Jaiswal, P.; Gao, Y.F.; Rahmati, M.; Vanderborght, J.; Simunek, J.; Vereecken, H.; Vrugt, J.A. Parasite inversion for determining the coefficients and time-validity of Philip's two-term infiltration equation. *Vadose Zone J.* **2022**, *21*, e20166. [CrossRef]
38. Selker, J.S.; Duan, J.; Parlange, J.Y. Green and Ampt infiltration into soils of variable pore size with depth. *Water Resour. Res.* **1999**, *35*, 1685–1688. [CrossRef]

39. Xie, C.K.; Cai, S.Z.; Yu, B.Q.; Yan, L.B.; Liang, A.Z.; Che, S.Q. The effects of tree root density on water infiltration in urban soil based on a Ground Penetrating Radar in Shanghai, China. *Urban For. Urban Green.* **2020**, *50*, 126648. [CrossRef]
40. Khasraei, A.; Abyaneh, H.Z.; Jovzi, M.; Albaji, M. Determining the accuracy of different water infiltration models in lands under wheat and bean cultivation. *J. Hydrol.* **2021**, *603*, 127122. [CrossRef]